ELSEVIER

Spectrochimica Acta Part B 57 (2002) 1753–1770

SPECTROCHIMICA ACTA PART B

www.elsevier.com/locate/sab

Studies about the origin of the non-spectroscopic interferences caused by sodium and calcium in inductively coupled plasma atomic emission spectrometry. Influence of the spray chamber design

Salvador Maestre, Juan Mora, José-Luis Todolí*

Department of Analytical Chemistry, University of Alicante, P.O. Box 99, 03080, Alicante, Spain

Received 22 April 2002; accepted 16 August 2002

Abstract

In the present work a systematic study about the characterization of the performance of three spray chambers in terms of inductively coupled plasma atomic emission spectrometry (ICP-AES) analytical figures of merit and matrix effects caused by sodium and calcium at high concentrations was carried out. In addition, experiments were conducted in order to understand the origin of the non-spectroscopic interferences caused by sodium and calcium in ICP-AES. The chambers used were a double pass (DP) a cyclonic (CC) and a home made single pass (SP). In all the cases a high efficiency nebulizer was operated at liquid flow rates ranging from 20 to 200 μl min^{-1}. The results revealed that the ICP-AES sensitivities were higher for the SP than for the two remaining spray chambers. The data concerning the matrix effects caused by concomitants (i.e. sodium and calcium) indicated that the extent of these effects was higher for the DP than for the SP and CC. In the presence of these elements in excess, finer tertiary aerosols were generated than for water. Nonetheless, similar primary aerosols were generated irrespective of the matrix tested. Several experiments were conducted in order to elucidate the mechanism leading to the matrix effects caused by sodium and calcium in terms of aerosol transport towards the plasma. It was concluded that a combination of droplet charge effects and a reduction in the extent of solvent evaporation could be responsible for these effects.

Keywords: Inductively coupled plasma atomic emission spectroscopy; Non-spectroscopic interferences; Spray chamber; Easily ionized elements

1. Introduction

In inductively coupled plasma atomic emission spectrometry (ICP-AES), the analytical signal and the extent of the matrix effects depend mainly on the amount of sample that is introduced into the plasma. When dealing with liquid samples, the sample is usually turned out into an aerosol (primary aerosol) and only the finest droplets are driven towards the plasma (tertiary aerosol). The emission signal is given by both the amount and the characteristics of the tertiary aerosol. These

*Corresponding author. Fax: +34-96-590-3464.
E-mail address: jose.todoli@ua.es (J.-L. Todolí).

0584-8547/02/$ - see front matter
PII: S0584-8547(02)00141-6

parameters are, in turn, a strong function of the design and performance of the sample introduction system. The most usual liquid sample introduction system consists of a nebulizer, which generates the aerosol, and a spray chamber, which selects the maximum drop size introduced into the plasma [1].

Regarding spray chambers, the double pass spray type one (also called Scott type) has been traditionally the most common design used in the ICP instruments [2]. Additional spray chamber designs such as the cyclonic [3–6] or the single pass [7,8] can be found in the literature. It has been described that, in the case of cyclonic spray chambers, the aerosol follows a double concentric spiral trajectory before being introduced into the plasma base [9]. However, according to recent mathematical simulations [10,11], these chambers appear to behave primarily as an impactor rather than an industrial cyclonic device. What seems clear is that the aerosol path can be considered to be easier for single pass than for cyclonic or double pass designs. In addition, modifications of the cyclonic design have been developed in order to handle low volume samples [12–14], to interface separation techniques with plasma spectrometry [15] and to analyze samples by flow injection analysis [8,16].

Matrix effects due to easy and not easy-to-ionize elements (e.g. sodium or calcium) have been recently reviewed [17]. These matrix effects can be originated inside the plasma and/or in the liquid sample introduction system. As regards the effects in the plasma, sodium and calcium can modify the plasma local values of temperature and electronic density. Other processes such as modification in the spatial distribution of the emitting species have also discussed as possible sources of the matrix effects [17]. It is well known that, in order to minimize the interferences due to the modification of plasma thermal characteristics, it should be operated under the so-called robust conditions [18]. These conditions are reached when working at high RF power values (i.e. higher than 1.3 kW more or less) and at low nebulizer gas flow rates (i.e. below 0.7 l min^{-1}).

As regards the contribution of the sample introduction system to the matrix effects caused by concomitants, it should be stated that, although this factor was initially neglected [19,20], the presence of high concentration of elements in the sample may have a significant influence on the behavior of this component of the equipment [21,22]. Under plasma robust conditions, the matrix effect caused by elements such as sodium or calcium are mainly attributed to the sample introduction system [23]. In general terms, when dealing with samples with concomitant concentrations below 20 000 mg l^{-1}, the nebulization process is not disturbed. However, the mass of analyte transport rate leaving the spray chamber can be modified with respect to that found for plain water solutions [21,23]. A phenomenon responsible for changes in the total mass of analyte reaching the plasma when having a highly concentrated element in the sample is the so called aerosol ionic redistribution, AIR. This accounts for the changes in the analyte concentration in the aerosol droplets when compared to the concentration in the original sample bulk [24,25]. According to the bibliography, AIR takes place when a new droplet is generated (i.e. nebulization or renebulization processes inside the spray chamber due to droplet impacts) [26]. Droplet charge effects can play a relevant role on the extent of the AIR through the droplet Coulombic fission processes [27–29]. Another phenomenon responsible for the modification in the total amount of analyte reaching the plasma is the solvent evaporation. In the presence of dissolved salts, this event is dampened with respect to water [30,31]. Moreover, for other ionic matrices (i.e. inorganic acids) it has been observed that the solvent evaporation from the solution settled on the spray chamber walls affects the extent of the interferences [32].

The design of the spray chamber has an important effect on the extent of the interferences in ICP-AES, because it modifies the magnitude of the aerosol transport phenomena taking place along its path towards the plasma. Previously published work has already shown that for a cyclonic spray chamber the suppression in the emission signal caused by inorganic acids is less significant than for a double pass spray chamber [33,34].

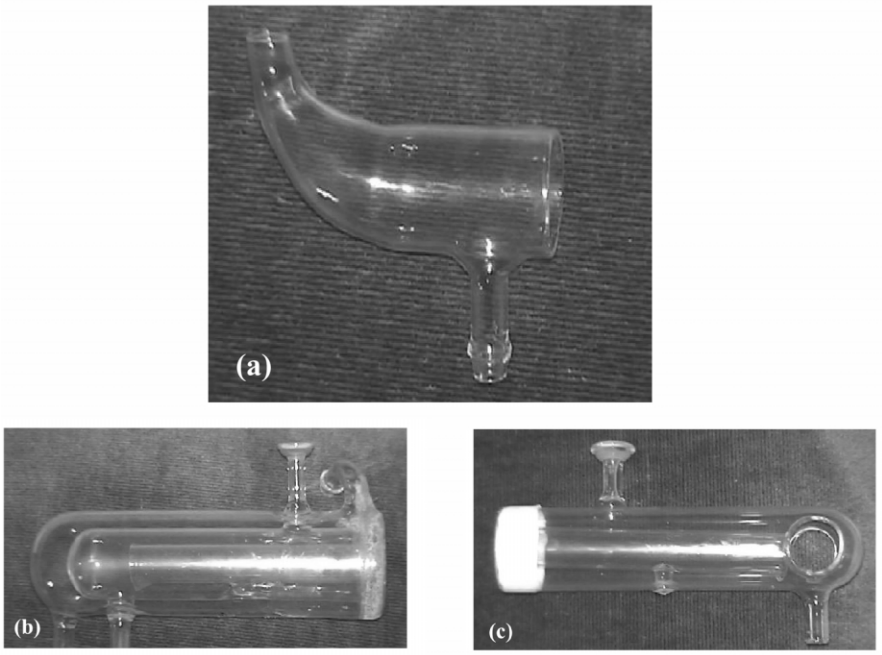

Fig. 1. Pictures of different spray chambers. (a) The single pass spray chamber, SP; (b) jacketed double pass spray chamber, JDP; (c) orifice double pass spray chamber, ODP.

The present work will be focused on the study of the influence of the spray chamber design on the ICP-AES analytical figures of merit and the matrix effects due to the presence of high concentrations of sodium and calcium in the sample. In addition, fundamental studies aimed to the understanding of the mechanism responsible of the matrix effects in terms of aerosol transport towards the plasma will be presented in this work.

2. Experimental

A high efficiency pneumatic concentric nebulizer [35], HEN (HEN-170-AA, J.E. Meinhard CA, USA) was used throughout. Its gas outlet cross-section area was 1.1×10^{-2} mm^2, whereas its free aspiration rate was 40 μl min^{-1} at 1 l min^{-1} argon stream.

Four spray chambers were used, a Ryton double pass-Scott type spray chamber (DP, Perkin-Elmer Überlingen, Germany), a glass cyclonic spray chamber (CC, Glass Expansion, Pty, Australia), a homemade single pass spray chamber (SP, see picture in Fig. 1a) and a jacketed double pass spray chamber (JDP, see picture in Fig. 1b). In all the cases, tertiary aerosols left the spray chamber by an upper exit, whereas drain (i.e. coarsest droplets) was removed via a lower conduction. The inner volumes were 100, 43, 22 and 105 cm^3 for the DP, CC, SP and the JDP, respectively. In the experiments carried out with the JDP, the chamber walls temperature was controlled by means of a thermostated bath (Haake, Mod. F3-K Haake Mess-Technik GmbHu Co., Karlsruhe, Germany). The temperatures of the spray chambers walls were settled at 0, 15, 25 and 50 °C.

In order to measure the aerosols inside the chamber, a home made double pass spray chamber with an orifice was used (ODP, see picture in Fig. 1c). Its inner volume was 100 cm^3. Obviously, the chamber orifices modified the gas dynamics, but they were expected not to cause any change in the aerosol transport phenomena inside the chamber central tube.

The liquid sample was supplied to the nebulizer by means of a Gilson Minipuls 3 peristaltic pump (Villiers Le Bel, France). The liquid flow rate (Q_l) was varied between 20 and 200 μl min^{-1} by using 0.19-mm i.d. Tygon capillaries. Argon was employed for nebulization in all the cases.

The drop size distributions (DSD) of the aerosols generated by the nebulizer (primary aerosols) and those leaving the spray chamber (tertiary aerosols) were characterized by means of a laser Fraunhofer diffraction system (model 2600c, Malvern Instruments, Malvern Worcestershire, UK). The laser beam generated by this instrument has a 10-mm diameter. Because primary aerosols were characterized by placing the nebulizer tip at 10 mm from the beam center, droplets included within the 5–15-mm range from the nebulizer exit were measured. In the case of the tertiary ones, the exit of the spray chamber was placed 5 mm away from the laser beam center. Therefore, the droplets which interacted with the laser beam were those contained up to 10 mm above the spray chamber exit. When the ODP was used, the laser beam went through the orifice located near the end of the centered tube. A set of three replicates was performed in each case, the precision (R.S.D.) achieved being always lower than 2%.

Solvent transport rate (S_{tot}) measurements were performed by means of a direct method (i.e. by the adsorption of the aerosol in a U-tube filled with silica gel during a period of 10 min). By weighing it before and after the aerosol tube exposition, the S_{tot} values were easily derived. Analyte transport rate values were obtained by a direct method (i.e. by collecting the aerosol on a glass fiber filter, type A/E, 47-mm diameter, 0.3-μm pore size, Gelman Sciences, Ann Arbor, MI, USA). To this end, a 500-mg l^{-1} Mn solution was nebulized. The Mn retained after a period of 10 min was extracted by washing the filters with 1.0% (w w^{-1}) nitric acid solution. The total solution volume was made up to 100 ml in a volumetric flask. Finally, the Mn concentration in each solution was determined by flame atomic absorption spectrometry (FAAS). The precision of the transport experiments was always better than 5% (R.S.D. from three replicates).

Table 1
ICP-AES operating conditions

RF power (kW)	1.45
Integration time (ms)	100
Sampling time (ms)	1000
Outer gas flow rate (l min^{-1})	15
Auxiliary gas flow rate (l min^{-1})	0.5
Nebulizer-carrier gas flow rate (l min^{-1})	0.6
Observation height (mm above load coil)	5
Sample uptake rate (ml min^{-1})	Variable
Injector diameter (mm)	0.87

The emission signal was measured with a Perkin-Elmer Optima 3000 ICP-AES instrument (Überlingen, Germany). Table 1 gathers the conditions of the instrument. The viewing height, RF power and carrier gas flow rate were optimized for each chamber in order to obtain the highest Mg II/Mg I ratio.

Aqueous standards containing 10 mg l^{-1} of each element were prepared from an ICP multielement standard solution (IV, Merck, Darmstadt, Germany). Table 2 lists the wavelengths and line energy sum values, E_{sum} (i.e. sum of ionization and excitation energies) for ionic lines as well as the excitation energy values for the atomic ones. Solutions of sodium and calcium were prepared from solid NaCl and $CaCl_2$ (Panreac, analysis grade). In order to prevent the nebulizer tip blocking induced by solid particles, every solution was previously filtered using PTFE filters (1-μm pore size, Millipore).

3. Results and discussion

3.1. Preliminary considerations

The system used in the present work to measure the aerosol drop size distributions has a detector which consists of a series of 30 concentric rings placed on the lens focal plane [36]. Fig. 2 plots the energy measured by the detector rings for two droplets having different diameters. According to this figure, for a small droplet, the laser radiation is preferentially scattered and focused on the rings 21–30 (i.e. high angles) whereas for a coarse one, the majority of the radiation does on the two first rings (i.e. low angles).

Table 2
Lines tested in the present work

Line	Wavelength (nm)	E_{sum}[a] (eV)
Li I	670.781	1.8
Mn I	294.920	2.8
Mg I	285.213	3.1
Cr I	357.869	3.5
Cu I	324.754	3.8
Al I	308.215	4
Ga I	294.364	4.31
Pb I	216.999	5.7
Cu I	222.778	7.2
Cd I	361.061	7.4
Zn I	334.502	7.8
Ba II	455.403	7.93
Sr II	421.552	8.6
Sr II	407.771	8.7
Ba II	230.424	11.2
Mg II	280.270	12.1
Mn II	257.610	12.3
Cr II	267.595	12.9
Co II	228.616	13.7
Ni II	221.647	14.3
Cd II	226.502	14.5
Zn II	202.548	15.5
Mg II	279.079	16.5

[a] E_{sum} = Ionization energy + excitation energy.

Radiation that has passed through the aerosol without suffering diffraction reaches the detector center. By comparing this radiation with that measured in absence of aerosol, it is possible to estimate the amount (mass, volume) of aerosol which is being measured. The parameter obtained in this way is the so-called obscuration. Nevertheless, it is necessary to take into account the contribution of the drop size to the diffraction efficiency. To this end, the so called volume concentration (VC) can be used. The VC is defined as the percentage of laser sampling volume which is occupied by aerosol particles. This parameter is given by the following mathematical relationship:

$$\mathrm{VC} = \frac{100\log_e(1-Ob)}{\frac{-3}{2}b\sum\frac{V_iQ_i}{d_i}} \quad (1)$$

Where b is the length of the laser cylinder which is being used to obtain the diffraction pattern, Ob is the obscuration defined as the difference between the total laser energy and the scattered energy; d is the droplet diameter, V is the drop volume and Q a parameter directly related with the efficiency of diffraction.

Fig. 3 plots both the obscuration and the VC vs. the time for the tertiary aerosols generated when switching from water to a 5000 mg l^{-1} sodium solution. In this case, the HEN was coupled to a double pass spray chamber. The registered values of these magnitudes were lower than the optimum ones recommended by the manufacturer [37]. However, as shown in Fig. 3, the precision found was good. As it can be seen, while both solutions gave rise to similar values of the VC, the value of obscuration was larger for the aerosol corresponding to the sodium solution. Note that, under the conditions summarized in Fig. 3, the median of the tertiary aerosol volume drop size distribution (i.e. D_{50}) were 1.5 and 2.6 μm in the presence and in absence of sodium, respectively. This result meant that tertiary aerosols were finer for the sodium solution. According to these data, and those discussed in Fig. 2, the high proportion of fine droplets, instead of the increase in the aerosol volume, could be the responsible for the increase in obscuration when switching from water to a sodium solution. Therefore, the VC seemed to be a more appropriate parameter than the *Ob* in order to monitor any change in the volume of liquid aerosol reaching the plasma.

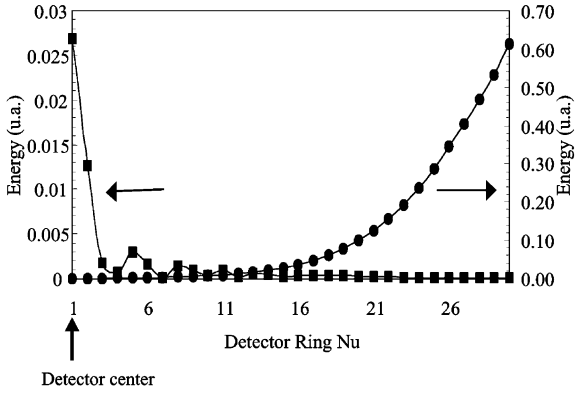

Fig. 2. Energy measured for two droplets with different diameters as a function of the detector ring. (-■-) Drop diameter: 118 μm; (-●-) Drop diameter: 1.2 μm.

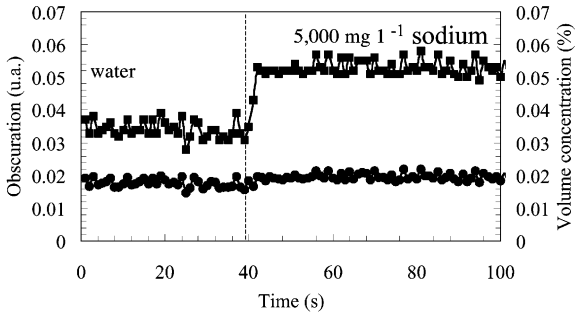

Fig. 3. Variation of the VC (-●-) and the obscuration (-■-) of the aerosols leaving the double pass spray chamber with time when switching from water to a 5000-mg l^{-1} sodium solution. $Q_g = 0.4$ l min^{-1}; $Q_l = 800$ μl min^{-1}.

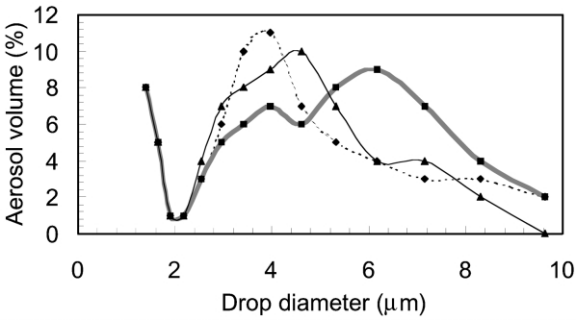

Fig. 4. Tertiary aerosol volume drop size distribution curves in frequency for the different chambers tested. Dashed line: cyclonic spray chamber, CC; black line: single pass spray chamber, SP; gray line: double pass spray chamber, DP. $Q_g = 0.4$ l min^{-1}; $Q_l = 50$ μl min^{-1}.

3.2. Plain water solutions

3.2.1. Aerosol characterization

Fig. 4 shows the complete tertiary aerosol volume drop size distribution curves for the CC, DP and SP spray chambers in a frequency representation. It can be observed that the three spray chambers gave rise to similar tertiary aerosols in terms of fine droplets. In every case, the whole tertiary aerosol volume was contained in droplets with diameters lower than 11.1 μm. This result could be explained according to the fact that the nebulization conditions led to a very low sample to gas flow rate ratio, thus favoring the generation of fine primary aerosols. Thus, almost the totality of the liquid volume of the primary aerosol was contained in droplets with diameters lower than 15 μm.

For a fine enough primary aerosol, the spray chamber design would play a secondary role and tertiary aerosols would be similar irrespective of the chamber used. However, it has been indicated that when working at conventional liquid flow rates (i.e. in the order of ml min^{-1}) even those droplets having very low diameters (i.e. <1 μm) are inefficiently transported through the spray chamber [38]. This effect appears to be directly related with the drop coalescence. Therefore, in order to reach a high transport efficiency, the aerosol drop number density should be low. Fig. 5 plots the drop size distributions for the primary aerosols generated by the HEN at two liquid flow rates. If we assume that two chambers are used which remove from the primary aerosol all the droplets having diameters higher than 10 and 20 μm in diameter, when operating the nebulizer at high sample flow rate (curve A), the aerosol volume leaving the chamber will be strongly influenced by its design. However, when the sample flow rate is lowered down to 100 μl min^{-1} (curve B), almost the same aerosol liquid volume would be contained in droplets below the maximum tertiary aerosol drop diameter for both chambers. Therefore, the chamber would not modify in a significant way the characteristics of primary aerosols. Furthermore, as it has been indicated in previous work, coagulation of droplets, leading to the generation of coarse droplets, is less severe at

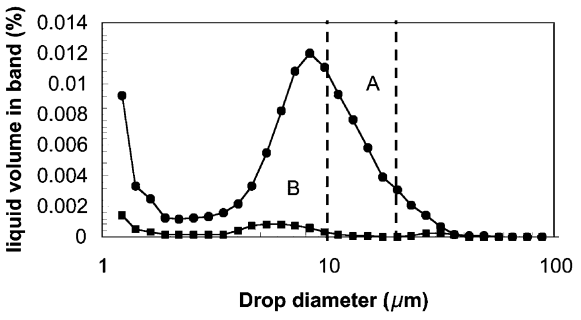

Fig. 5. Primary aerosol volume drop size distribution curves in frequency for the high efficiency nebulizer. (a) $Q_l = 800$ μl min^{-1}; (b) $Q_l = 100$ μl min^{-1}; $Q_g = 0.4$ l min^{-1}.

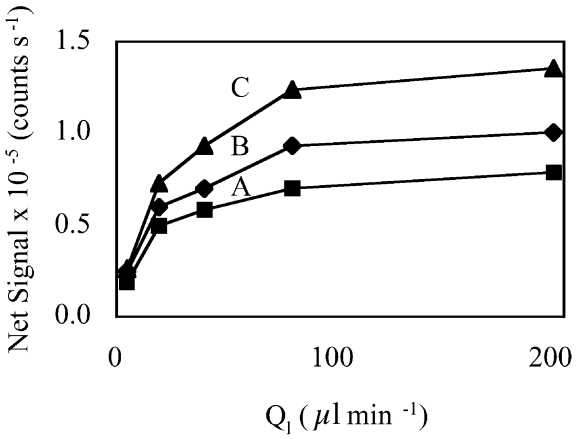

Fig. 6. Mn (257.610 nm) net emission intensity vs. the liquid flow rate for the three spray chambers tested. (a) Double pass spray chamber, DP; (b) cyclonic spray chamber, CC; (c) single pass spray chamber, SP. $Q_g = 0.6$ l min^{-1}.

low liquid flow rates and the solvent evaporation, leading to the generation of fine droplets, is more significant at low liquid flow rates [39].

3.2.2. ICP-AES analytical figures of merit

Fig. 6 shows the Mn (257.610 nm) emission intensities obtained for three spray chambers. Two features could be pointed out from this figure, the first one was that the SP gave rise to higher signals than the DP. These data agreed with the VC of the tertiary aerosols. Thus, at 50 μl min^{-1}, the VC were 0.02 and 0.04% for the DP and SP, respectively. For the latter chamber, the aerosol path towards the plasma was easier than for the two remaining chambers. The second one was that the signal for the different chambers became more similar as the sample flow rate decreased [40]. As it was previously pointed out, this trend can be related to the generation of finer primary aerosols that were more easily transported through the spray chamber. Moreover, the solvent evaporation from the aerosol also plays a very important role. At low liquid flow rates, solvent evaporation is expected to be very intense in relative terms. As a result, droplets could reduce their diameters below the spray chamber cut-off diameter thus being efficiently transported towards the plasma. Note that, as stated before, droplet coagulation becomes less severe as the liquid flow rate decreases. These factors made the contribution of the spray chamber design to be less significant at low liquid flow rates.

The detection limits found for the SP, CC and DP are presented in Table 3. The detection limits have been obtained by applying the 3 s_B criterion, where s_B corresponds to the standard deviation obtained from 20 blank signal replicates. As it can be seen, the detection limits supplied by the different spray chambers are of the same order of magnitude. The SP presented a noisy background signal that, in some cases, counterbalanced the higher sensitivities found with respect to the two remaining chambers.

To monitor the plasma thermal properties several parameters have been proposed in the literature. Among them the ionic-to-atomic emission intensity ratios for a suitable element. Magnesium is the most widely accepted element to carry out this kind of study [41], although additional elements, as chromium have also been chosen [42,43]. In the present work the ratios for both elements were obtained and their values were multiplied by a

Table 3
Limits of detection for the three spray chambers tested and several lines[a]

	LOD (mg l^{-1})		
	SP	CC	DP
Zn 202.548	0.03	0.013	0.008
Ni 221.647	0.03	0.02	0.008
Cu 222.778	0.06	0.11	0.05
Cd 226.502	0.010	0.006	0.008
Co 228.616	0.03	0.04	0.07
Ba 230.424	0.02	0.02	0.03
Cr 267.716	0.02	0.004	0.03
Mn 257.610	0.009	0.007	0.004
Mg 279.079	0.2	0.06	0.08
Mg 280.270	0.003	0.002	0.002
Mg 285.213	0.007	0.002	0.006
Mn 294.920	0.009	0.012	0.02
Al 308.215	0.17	0.15	0.07
Cu 324.754	0.02	0.010	0.02
Cr 357.869	0.4	0.12	0.11
Cd 361.061	0.4	0.4	0.4
Ba 455.403	0.004	0.002	0.002
Li 670.781	0.013	0.006	0.04

[a] $Q_g = 0.6$ l min^{-1}; $Q_l = 200$ μl min^{-1}.

factor taking into account the difference in the detector response as a function of the wavelength. Under the conditions tested, all the spray chambers gave rise to similar values of the Mg II/Mg I and Cr II/Cr I ratios. At 200 μl min^{-1} and 0.6 l min^{-1}, the values of the Mg II/Mg I ratio were 7.6 and 8.0 for the DP and SP, respectively. The respective values of the Cr II/Cr I ratio were 11.4 for both spray chambers. Therefore, the use of a single pass spray chamber that allowed a higher amount of aerosol to reach the plasma did not affect the plasma excitation properties.

Fig. 7a shows the Ar signal recorded for the DP, the CC and the SP at different sample flow rates. For all these designs, an increase in the amount of sample nebulized gave rise to higher Ar signals. In previous reports it has been indicated that this trend reveals an enhancement of the plasma thermal conductivity [44,45]. However, when comparing the different chambers, it can be seen that for the CC lower argon emission intensities were found than for the DP whereas the SP afforded intermediate values of this signal. According to previous studies [33,34], at liquid flow rates above 0.4 ml min^{-1}, cyclonic spray chambers give rise to higher solvent transport rates than double pass ones. Fig. 7b shows the variation of the OH band emission intensity for the three spray chambers tested vs. the sample flow rate. If the plasma characteristics are not significantly modified, this signal can be considered as a good indicator of the mass of solvent reaching the plasma. As expected, the OH band emission signal was higher for the cyclonic spray chamber than for the double pass one. The SP supplied values of the OH signal similar to those found for the CC, although this variable was slightly higher for the SP, at least at the lowest liquid flow rates tested. Finally, from Fig. 7b, it could be observed that the higher the sample flow rate, the higher the OH emission signal for all the chambers.

As regards the wash-out time, defined as the time required for the signal to reach a 1% of the steady-state value [14,46]. Table 4 shows the values of this parameter for the DP, the CC and the SP at two different liquid flow rates. As it can be seen from this table, wash-out times were longer for the double pass pray chamber than for the cyclonic one. This fact has been related to the bigger inner volume of the double pass design and the tortuous aerosol path inside it. Meanwhile, the SP afforded the lowest values of this parameter. Obviously, the lower the sample flow rate the longer the wash-out time. Finally, from data of Table 4, it was also clear that the differences between the spray chamber were enhanced at low sample flow rates.

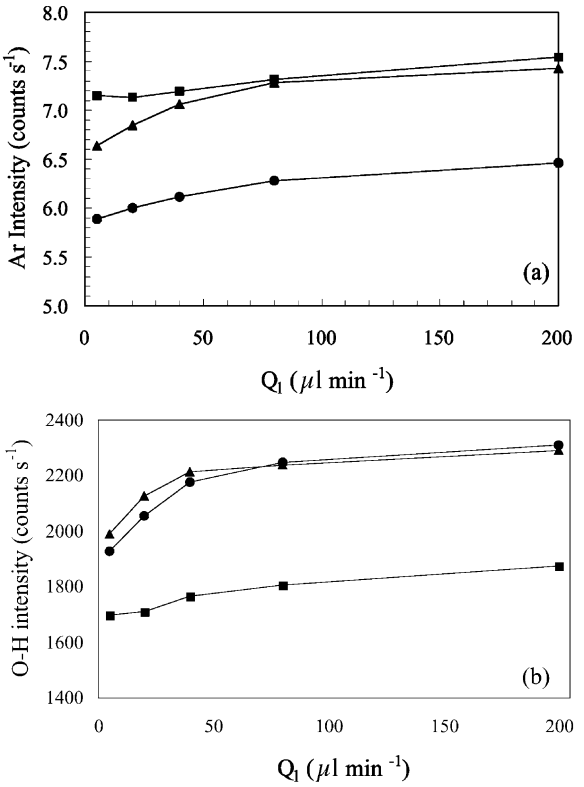

Fig. 7. Ar (a) and OH band (b) emission signal vs. Q_l. (■) Double pass spray chamber, DP; (●) cyclonic spray chamber, CC; and (▲) single pass spray chamber, SP. $Q_g = 0.6$ l min^{-1}.

3.3. Steady-state matrix effects caused by concomitants

3.3.1. Tertiary aerosol drop size distribution

In order to evaluate the effect of the spray chamber on the change in tertiary aerosols induced by the presence of sodium, the accumulated per-

Table 4
Wash-out times[a] at different sample flow rates for two elements and the three chambers tested

Chamber	Q_l/μl min^{-1}	Wash out time, Mg (s)	Wash out time, Cu (s)
DP	50	95	89
DP	200	273	253
CC	50	60	56
CC	200	197	182
SP	50	44	47
SP	200	136	107

[a] Defined as the time elapsed until the signal drops down to a 1% of its steady-state value.

centages for sodium were divided by those for water. Fig. 8 plots the relative accumulated volume vs. the drop diameter for the three chambers tested. In this case, this relative parameter was calculated according to:

$$\%\ \text{relative accumulated volume} = \frac{(\text{Accumulated volume})_{\text{sodium}}}{(\text{Accumulated volume})_{\text{water}}} \times 100 \qquad (2)$$

The relative accumulated volume gave us an indication about the drop size range at which the effect of sodium was more significant. From Fig. 8, it can be observed that, as expected [27–29], finer tertiary aerosols were obtained for sodium than for pure water. Furthermore, the effect of the presence of sodium was much more noticeable for droplets with diameters lower than 1.2 μm. For those droplets, the relative aerosol liquid volume was about two times higher in the presence of sodium than for water. From the data shown in Fig. 8, it was also possible to conclude that sodium modified in a more noticeable way the tertiary aerosols (i.e. higher relative accumulated volumes) in the case of the DP than for the CC and the SP.

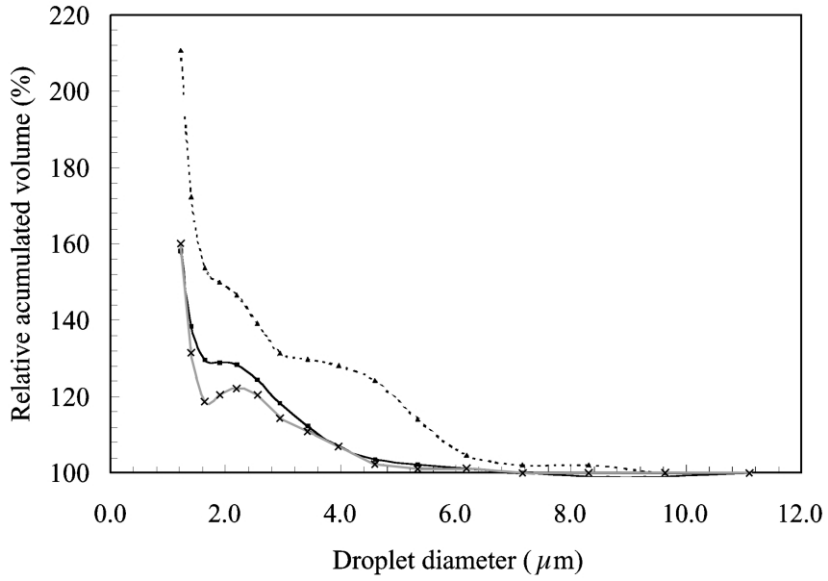

Fig. 8. Relative accumulated volume percentage (see text for explanation) vs. drop diameter for the tertiary aerosols and the chambers tested. Dotted line: double pass spray chamber, DP; black line: cyclonic spray chamber, CC; gray line: single pass spray chamber, SP. $Q_g = 0.4$ l min^{-1}; $Q_l = 50$ μl min^{-1}.

For the two latter devices, the presence of sodium did not have any significant effect for those droplets with diameters above 7.2 μm (i.e. relative accumulated volume values close to 100%) whereas for the double pass spray chamber this diameter was located at 9.6 μm.

As regards the VC, there were no conspicuous differences as a function of the solution tested. Thus, for the DP, at $Q_g = 0.4$ l min^{-1} and $Q_l = 50$ μl min^{-1}, this magnitude took values of 0.02% both for water and sodium 5000 mg l^{-1} solution. The respective VC values in the case of the SP were 0.04 and 0.045%.

3.3.2. Studies about the mechanism responsible for the matrix effects

The tertiary aerosols were finer when an ionic matrix was present in the sample than when nebulizing water alone. A possible explanation was given by Agnes and co-workers as follows [27–29]: Pneumatically generated droplets can have a net electrical charge at their surfaces. Once droplets are generated, they reduce their diameters through solvent evaporation. When these droplets reach a critical diameter (approx. 4 μm) [28] they cannot withstand the charge on their surfaces and they are dispersed in other progeny ones.

In the present work, the effect of the presence of sodium on the characteristics of tertiary aerosols was evaluated. The experiments were aimed to modify the extent of two processes: (i) the solvent evaporation; and (ii) the net electrical charge at the surface of the droplets.

Tertiary aerosols were measured at different temperatures. The matrix used was 5000 mg l^{-1} of either Na or Ca solutions. The jacketed double pass spray chamber spray chamber (JDP) was used (see Fig. 1b). For a given set of nebulization conditions (i.e. sample and gas flow rates) the matrix effects in terms of shift in drop size distribution were more severe as the temperature went up. For instance, at 0.4 l min^{-1} and 800 μl min^{-1}, the drop in D_{50} induced by the presence of sodium or calcium was 25 and 80% at 0 and 50 °C, respectively. These results were in agreement with the theory proposed by Agnes et al., because an increase in the chamber walls temperature promoted the solvent evaporation and it could lead to an increase in the droplet fission frequency.

From the comments made before, it appears that the matrix effects were more severe as the solvent evaporation was enhanced. The extent of solvent evaporation could also be modified by changing the nebulization conditions. At this point additional experiments were carried out at room temperature by modifying the nebulizer liquid and gas flow rates. Thus, for example, for the SP at a 0.4l min^{-1} gas flow rate, the D_{50} dropped by 42% and 13% at 50 and 800 μl min^{-1}, respectively. Therefore it was obvious that the matrix effects were more severe as the liquid flow rate was decreased. Again this trend fitted well with the mechanism proposed by Agnes et al. However, when increasing the nebulizer gas flow rate (i.e. enhanced the solvent evaporation) the matrix effects caused by either sodium or calcium were less severe. Thus, at a liquid flow rate of 800 μl min^{-1}, the presence of sodium induced a 13 and 2% drop in the D_{50} at a gas flow rate of 0.4 and 1.0 l min^{-1}, respectively. These latter results were not in agreement with the droplet fission theory and were consistent with previous investigations which indicate that the matrix effects caused by inorganic acids are more severe at low than at high gas flow rates [47].

In the explanation proposed by Agnes and coworkers, the solvent evaporation is of capital importance. However, this aerosol transport phenomenon can be considered as relatively slow. It has been indicated that those droplets having diameters higher than 10 μm need approximately 60 s to evaporate completely at room temperature [30,31]. According to simple theoretical calculations, based on previously published work [30,31], it was observed that the time required for the complete evaporation of a droplet with a 1-μm diameter is approximately 60 ms. We could also roughly estimate the minimum time that a droplet will spend inside the double pass spray chamber by dividing the gas flow rate by the inner volume of this chamber. At 0.7 l min^{-1} the droplet residence time in the DP chamber is approximately 9 s. For plain water droplets having 1- and 10-μm initial diameters, the former would evaporate completely (the evaporation time for that droplet would

be 60 ms) whereas for the latter droplet, the final diameter after 9 s would be 9.5 μm. Therefore, theoretically, the change in drop size for coarse droplets due to evaporation would be almost negligible. Note that in these calculations, the contribution of the increasing gas saturation degree caused by the progressive solvent evaporation has been neglected. Besides this, it has also been mentioned that the critical diameter below which droplets disperse in other progeny ones is approximately 4 μm [27]. For a 5000 mg l^{-1} sodium solution, the droplets that would reach this diameter through solvent evaporation for a 9-s residence time were those having approximately 5 μm in diameter. Therefore, according to these data, the main mechanism responsible for the generation of finer aerosols in the presence of inorganic species than for pure water does not appear to be the solvent evaporation and their further dispersion in finer droplets, at least at room temperature.

A possible explanation for the effect of sodium on tertiary aerosol characteristics could be the break down of those droplets having a charge–diameter ratio above a critical value just at the exit of the nebulizer. The primary aerosols were measured for water, sodium and calcium matrices at 5 mm from the nebulizer tip. These experiments revealed that, in the presence of either sodium or calcium at 5000 mg l^{-1}, the aerosols had the same statistical parameters as for water alone. Therefore, the aerosol differences as a function of the ionic matrix were due to processes occurring after the aerosol generation. Further experiments were carried out in which the aerosols characteristics were measured at 18 mm from the nebulizer tip and across the aerosol cone. These experiments were performed to investigate the effect of the aerosol solvent evaporation just after its generation. Again, the presence of sodium did not result in any significant change in the whole drop size distribution.

Water solutions containing sodium or calcium together with surfactants were prepared in order to decrease the net charge on the droplets and, hence, to decrease the fission's frequency during the transport of the aerosol through the spray chamber. To this end three surfactants of different ionic characteristics were used, a non-ionic surfactant (i.e. Triton X-100) an anionic surfactant (i.e. sodium dodecyl sulfate, SDS) and a cationic one (hexadecyl-tributylamonium bromide, CTAB). These compounds were present in the solution at a concentration corresponding to the critical micelle concentration (i.e. CMC). The results indicated that the presence of surfactant did not modify in a significant way the matrix effects caused by either sodium or calcium in terms of changes in the tertiary aerosol characteristics. At 50 μl min^{-1} and 0.4 l min^{-1}, the drops in D_{50} caused by the presence of sodium with respect of water were 45, 54 and 47% for Triton X-100, SDS and CTAB, respectively (remember that, in absence of surfactant, the drop in D_{50} was 42%). These results were not in agreement with a droplet fission mechanism.

Another experiment was carried out in order to find the part of the spray chamber in which the matrix effects were more significant. In this case, we used the double pass spray chamber shown in Fig. 1c (ODP). The aerosols were measured for water and for the 5000-mg l^{-1} sodium solution. At 0.2 l min^{-1} and 200 μl min^{-1}, the $D_{3,2}$ of the aerosols leaving the inner tube of the ODP were 18% lower in the presence of sodium than those measured for pure water. Therefore, it could be concluded that the changes in the aerosol characteristics induced by the presence of sodium were produced, at least partially, somewhere between the nebulizer tip and the exit of the spray chamber inner tube.

Stewart and Olesik [32] have concluded that the charge effects are not responsible for the generation of finer aerosols in the presence of ionic matrices such as nitric acid solutions. Solvent evaporation from the droplets surface can also be responsible of the changes in the characteristics of the tertiary aerosol induced by the matrix [30] because the vapor pressure of the solution decreases as increasing the salt concentration. Theoretical calculations [31] demonstrated that for a 10 000 mg l^{-1} sodium solution, the decrease in droplet diameter would be lower than 5% and 2.5% for droplets with diameters of 0.5 and 1 μm, respectively. This effect becomes less obvious as the salt concentration decreases. Finer tertiary aerosols could be expected in the presence of dissolved

salts than for a pure solvent. It must be pointed out that the finest droplets tend to evaporate faster than coarsest ones because there is an increased internal pressure due to the surface curvature. Therefore, for a pure solvent, small droplets tend to disappear through solvent evaporation whereas the coarsest ones still remain in the aerosol stream making the average size parameters to be larger (i.e. coarser aerosols). Since the presence of dissolved salts dampens the solvent evaporation, small droplets remain in the aerosol, thus giving rise to lower statistical mean diameters [30].

As it was demonstrated by the data discussed up to this point, the mechanism responsible for the modification in the characteristics of tertiary aerosols caused by sodium was not clear. Therefore, an experiment was done in order to evaluate the relative influence of the drop Coulomb fission processes and the reduction of the solvent evaporation on the sodium matrix effects. D_{50} of the aerosols leaving the double pass spray chamber were plotted vs. the sodium concentration. In order to carry out these experiments, the setup presented in Fig. 9a was used. It consisted of two vessels (one containing distilled water, 1, and another one containing a sodium 5000 mg l^{-1} solution, 2), a magnetic stirrer, a peristaltic pump and two independent capillaries. The HEN and a double pass spray chamber were used. At a given moment, the pump was switched on at 200 μl min^{-1}. As it can be seen in Fig. 9a, the solution pumped towards the nebulizer was that of vessel 1 (i.e. that initially having distilled water). Simultaneously, the 5000 mg l^{-1} sodium solution was aspirated from vessel 2 at the same flow rate and driven towards vessel 1. This system simulated a continuously stirred reactor, so that, the variation of the sodium concentration in vessel 1 vs. the time was easily obtained. Fig. 9b shows the variation of the D_{50} of the aerosols leaving the double pass spray chamber vs. the sodium concentration. The results showed that there was a steep decrease in the D_{50} vs. the sodium concentration down to a steady-state value. Interestingly, Fig. 9b shows that there were three different zones. A first one in which the D_{50} decreased very slowly as the sodium concentration increased up to approximately 900 mg l^{-1}, a second one in which the D_{50} drop was more pronounced and, finally a region (sodium concentrations higher than approx. 350 mg l^{-1}) in which a steady D_{50} was reached. As it is also represented in Fig. 9, these results could be explained as follows: at very low sodium concentrations, the Coulomb fission mechanism could be neglected, because the surface charge to droplet volume ratio was expected to be low. As a result, the slower solvent evaporation in the presence of sodium than for water could be the responsible of the very slight decrease in D_{50} with sodium concentration. As long as the sodium concentration increased, the solvent evaporation became less efficient and the charge at the surface of the droplets increased. In this situation the rate of the change of the D_{50} vs. sodium concentration increased, this behavior suggested us that the two

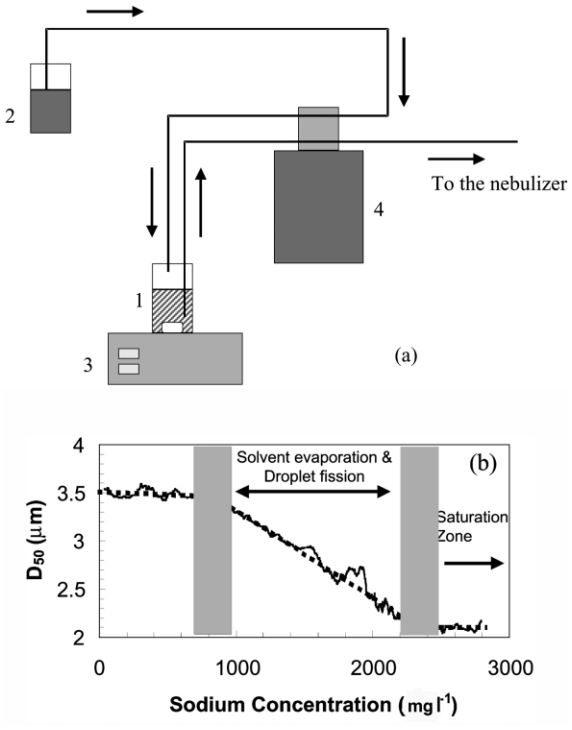

Fig. 9. Experimental setup employed to study the variation of the D_{50} of the tertiary aerosols vs. sodium concentration: (1) stirred reactor; (2) vessel containing the 5000 mg l^{-1} sodium solution; (3) magnetic stirrer; (4) peristaltic pump. (b) D_{50} of tertiary aerosols vs. the sodium concentration. $Q_l = 200$ μl min^{-1}; $Q_g = 0.6$ l min^{-1}. Double pass spray chamber, DP.

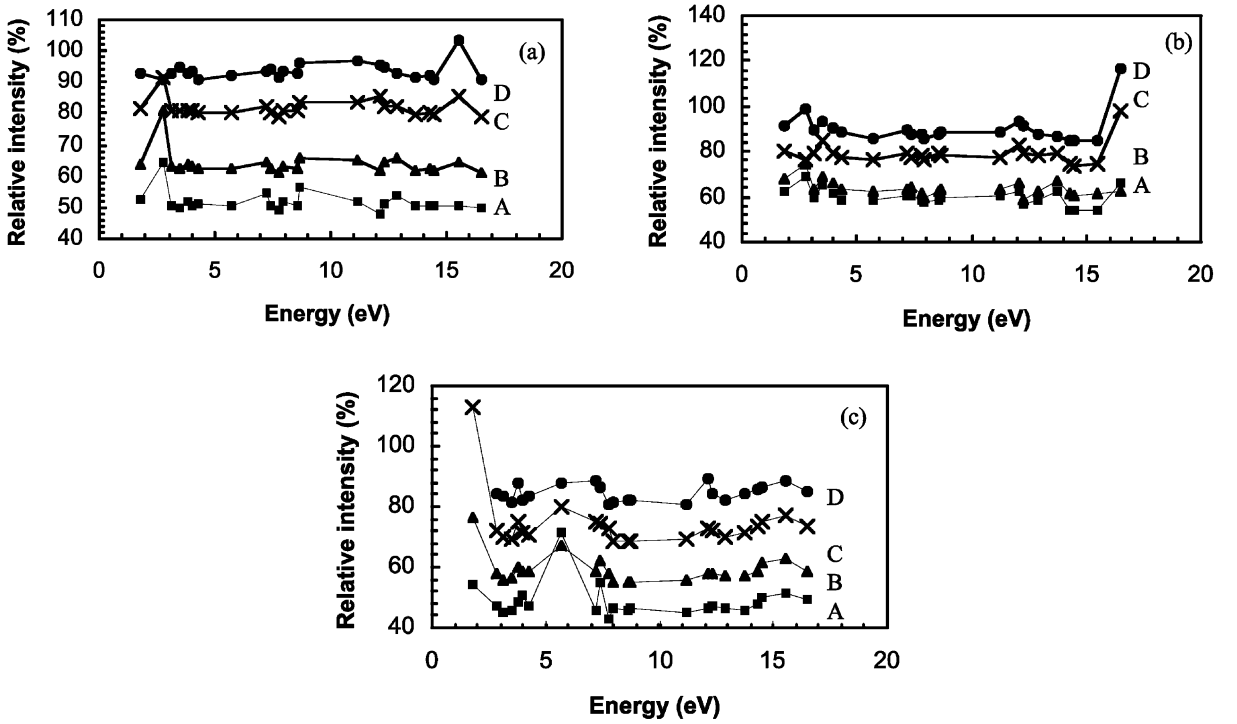

Fig. 10. Effect of the line energy on the relative net emission intensity (I_{rel}) for the cyclonic (a) the single pass (b) and the double pass (c) spray chambers. (A) $Q_l = 20$ μl min^{-1}; (B) $Q_l = 40$ μl min^{-1}; (C) $Q_l = 80$ μl min^{-1}; (D) $Q_l = 200$ μl min^{-1}. $Q_g = 0.6$ l min^{-1}. Matrix: sodium 5000 mg l^{-1}.

mechanisms (reduction in the solvent evaporation extent and Coulomb droplet fission) acted simultaneously. Finally, when the sodium concentration was further increased, a constant value in D_{50} was found. Therefore, a saturation effect was found in which the charge at the droplets surface reached a maximum value.

3.3.3. ICP-AES emission signal

Fig. 10 shows the effect of the excitation (atomic lines) and excitation + ionization energy (ionic lines) on the relative net emission intensity (I_{rel}) for the double pass (Fig. 10a), cyclonic (Fig. 10b) and single pass (Fig. 10c) spray chambers. The results summarized in this figure correspond to those using sodium as the concomitant and they have been obtained at four different liquid flow rates. I_{rel} has been calculated by dividing the emission intensity in the presence of sodium by that found in absence of this element. Finally, this parameter has been multiplied by 100. From these figures it can be seen that for a given liquid flow rate and spray chamber, I_{rel} did not vary in a significant way as a function of the line energy, for most of the lines. According to published results, this behavior is typical for a robust plasma [18]. Fig. 10 also shows that I_{rel} varied with energy line according to a pattern that was irrespective of the liquid flow rate. When switching between spray chambers, the pattern was just slightly modified. This can be accounted for by considering that there were no conspicuous differences in terms of the total mass of solvent delivered to the plasma for the chambers tested (Table 5). Finally, Fig. 10 shows that the I_{rel} values were somewhat lower (stronger matrix effects) for the double pass spray chamber than for the two remaining designs. The matrix effects found for calcium were slightly more pronounced than those discussed for sodium.

Table 5
Values of the total mass of solvent transported towards the plasma for the different spray chambers and matrices tested

Spray chamber	Q_l (μl min^{-1})	Matrix[a]	S_{tot} (mg min^{-1})
Double pass	20	Water	0.009
		Sodium	0.010
		Calcium	0.010
	200	Water	0.014
		Sodium	0.012
		Calcium	0.015
Cyclonic	20	Water	0.009
		Sodium	0.010
		Calcium	0.010
	200	Water	0.014
		Sodium	0.015
		Calcium	0.015

[a] The concentration of calcium or sodium is 5000 mg l^{-1}.

Nevertheless, as it can be seen in Table 5, S_{tot} for the two matrices tested were virtually identical.

The robustness of the plasma was also tested by measuring the Mg II/Mg I and the Cr II/Cr I ratios. It was found that none of these two parameters changed when introduced to either sodium or calcium solutions instead of introducing the plain water one. The conclusions drawn when measuring the argon atomic emission intensity measurements were also in agreement with those results.

Another striking effect is that observed at low Q_l, because the lower this variable the more severe the matrix effects. This fact, has been already discussed for inorganic acids and salts [48,49]. This fact could not be attributed to a change in the plasma excitation characteristics, because the ion-to-atom line ratios and the Ar signal registered did not agree with this trend. The measurements of the analyte transport rate leaving the spray chamber indicated that, at 20 μl min^{-1}, there was a slight drop in W_{tot} when sodium or calcium were present with respect to water. However, the drop in emission signal was, in all the cases, much more pronounced than that in analyte transport. Thus for example, for the double pass spray chamber, the Mn signal drop induced by the presence of sodium was approximately 10 and 50% at 200 and 20 μl min^{-1}, respectively. The respective W_{tot} dropping factors were just 6 and 18%. As it was verified in the present work, this lack of correspondence could not be attributed to the matrix effects caused by sodium when carrying out the W_{tot} determination through FAAS.

3.4. Transient matrix effects caused by concomitants

In previous studies concerning the effects of inorganic acids, it has been found that when switching between solutions of different acid concentration, an additional matrix effect appears; these are the so-called transient matrix effects. These dynamic interferences lead to an increase in the time required for the signal to reach a constant value [50–52]. The extent of the transient effects has been reported both in terms of emission signal and tertiary aerosol characteristics. According to Stewart and Olesik [32], when introducing a nitric solution after running the system with a more diluted acid solution, the signal sharply decreases and then increases slowly until it reaches a plateau. These effects have been explained by these authors in terms of preferential solvent evaporation form either the chamber walls or the aerosols. Among the variables influencing the acid transient effects, the spray chamber plays a very important role, mainly at low liquid flow rates. Thus, it has been found that the cyclonic spray chamber gives rise to a mitigation of these effects with respect to the double pass one [53]. In the present work, these effects have been characterized both in terms of changes in the tertiary aerosol drop size distribution and ICP-AES emission signal.

3.4.1. Tertiary aerosols

Fig. 11 plots the relative D_{50} vs. time for the double pass, cyclonic and single pass spray chambers. In these experiments distilled water was nebulized and, at a given moment (indicated by arrows in Fig. 11) a solution containing 5000 mg l^{-1} was introduced. The results indicated that it was necessary to wait approximately 5 s in order to reach the D_{50} steady value. Results found for calcium gave rise to identical drop size distribution profiles. According to the concentration of the concomitants, the solution physical properties were

not strongly modified. This could explain the differences when comparing these results with those found for inorganic acids [32].

3.4.2. Transient matrix effects on the ICP-AES signal

The evolution of the signal vs. time was registered when a solution containing 5000 mg l^{-1} of sodium was introduced after nebulization of a plain water solution. The results for the atomic line Cu 324 nm are presented in Fig. 12 for the double pass spray chamber. It can be easily checked that, at 200 μl min^{-1} there was no transient effect on the signal when the matrix of the solution was modified. Nevertheless, at 50 μl min^{-1} the situation was slightly different and the time required to achieve a stationary signal was approximately 20 s longer.

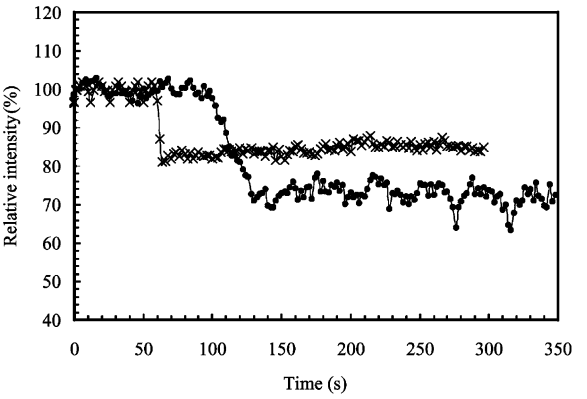

Fig. 12. Net emission signal for the Cu 324 atomic line vs. time when switching from a sample without matrix to a solution containing 5000 mg l^{-1} of sodium. (-X-) 200 μl min^{-1} and (-●-) 50 μl min^{-1}. Spray chamber: double pass. Q_g=0.6 l min^{-1}.

4. Conclusions

From the results shown in the present work, it can be concluded that the use of a single pass spray chamber for the introduction of very low liquid sample volumes in ICP-AES is beneficial from the point of view of either analytical figures of merit or matrix effects caused by sodium. It has also been observed that the work at very low liquid flow rates results in an intensification of the matrix effects caused by both sodium and calcium. This effect has proven to be independent of the spray chamber design.

The fundamental studies concerning the concomitant non-spectral interferences in ICP-AES indicated that while primary aerosols had the same characteristics irrespective of the matrix tested (i.e. water, sodium or calcium 5000 mg l^{-1}), tertiary aerosols were finer in the presence of any of these concomitants. Under the plasma conditions tested in the present work (i.e. robust plasma), the mechanism responsible for the changes in the tertiary aerosol would be a combination of a reduction in the extent of solvent evaporation and an increase in the droplet fission caused by electrostatic repulsion at the droplet surface in the presence of either sodium or calcium. These phenomena appear to take place simultaneously inside the chamber and their relative importance depends on the spray chamber design and nebulization conditions.

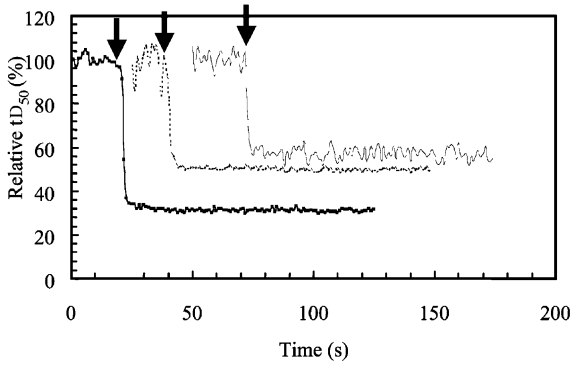

Fig. 11. Relative D_{50} of the aerosols leaving the chambers tested vs. time when switching from distilled water to a 5000 mg l^{-1} sodium solution. Q_g=0.6 l min^{-1}; Q_l=50 μl min^{-1}. (---) cyclonic, (-■-) double pass and (—) single pass spray chamber.

Acknowledgments

The authors wish to thank to Mr Alan Eastgate (Glass Expansion) for the loan of the cyclonic

spray chamber employed in the present study. Also the authors are grateful to the Dirección General de Investigación Científica y Técnica (DGICyT, Spain) for the economical support (Project Ref. 1FD 97-1080-C01 9.

References

[1] A. Montaser, M.G. Minnich, J. McLean, H. Liu, J.A. Caruso, C.W. McLeod, in: A. Montaser (Ed.), Inductively Coupled Plasma Mass Spectrometry, Wiley-VCH, New York, 1998, p. 83.

[2] R.H. Scott, V.A. Fassel, R.N. Kniseley, D.E. Nixon, Inductively coupled plasma-optical emission analytical spectrometry—compact facility for trace analysis of solutions, Anal. Chem. 46 (1974) 75–81.

[3] L. Ebdon, R. Collier, Particle size effects on kaolin slurry analysis by inductively coupled plasma-atomic emission spectrometry, Spectrochim. Acta Part B 43 (1988) 355–369.

[4] X. Zhang, H. Li, Y. Yang, Determination of impurities in highly pure platinum by inductively coupled plasma-atomic emission spectrometry, Talanta 42 (1995) 1959–1963.

[5] M. Hoenig, H. Baeten, S. Vanhentenrijk, G. Ploegaerts, T. Bertholet, Evaluation of various commercially available nebulization devices for inductively coupled plasma atomic emission spectrometry, Analysis 25 (1997) 13–19.

[6] M. Wu, G.M. Hieftje, New spray chamber for inductively coupled plasma spectrometry, Appl. Spectrosc. 46 (1992) 1912–1918.

[7] H. Isoyama, T. Uchida, T. Niwa, C. Iida, J.G. Nakagawa, Small spray chamber for inductively coupled plasma atomic emission-spectrometry and its evaluation by a digital signal sampling technique, J. Anal. At. Spectrom. 4 (1989) 351–355.

[8] H. Isoyama, T. Uchida, C. Iida, J.G. Nakagawa, Small spray chamber with a concentric nebulizer for inductively coupled plasma atomic emission-spectrometry, J. Anal. At. Spectrom. 5 (1990) 307–310.

[9] G. Lidén, A. Gudmundsson, Semi-empirical modelling to generalise the dependence of cyclone collection efficiency on operating conditions and cyclone design, J. Aerosol. Sci. 28 (1997) 853–874.

[10] G. Schaldach, L. Berger, H. Berndt, Meeting of the Federation of Analytical Chemistry and Spectroscopy Societies, Detroit, Paper # 18, 2001.

[11] G. Schaldach, L. Berger, I. Razilov, H. Berndt, Characterization of a cyclone spray chamber for ICP spectrometry by computer simulation, J. Anal. At. Spectrom. 17 (2002) 334–344.

[12] C. B'Hymer, K.L. Sutton, J. Caruso, Comparison of four nebulizer–spray chamber interfaces for the high-performance liquid chromatographic separation of arsenic compounds using inductively coupled plasma mass spectrometric detection, J. Anal. At. Spectrom. 13 (1998) 855–858.

[13] K.A. Taylor, B.L. Sharp, D.J. Lewis, H.M. Crews, Design and characterisation of a microconcentric nebuliser interface for capillary electrophoresis-inductively coupled plasma mass spectrometry, J. Anal. At. Spectrom. 13 (1998) 1095–1100.

[14] M. Haldimann, A. Eastgate, B. Zimmerli, Improved measurement of iodine in food samples using inductively coupled plasma isotope dilution mass spectrometry, Analyst 125 (2000) 1977–1982.

[15] J.A. Day, J.A. Caruso, J.S. Becker, H.J. Dietze, Application of capillary electrophoresis interfaced to double focusing sector field ICP-MS for nuclide abundance determination of lanthanides produced via spallation reactions in an irradiated tantalum target, J. Anal. At. Spectrom. 15 (2000) 1343–1348.

[16] M. Wu, Y. Madrid, J.A. Auxier, G. Hieftje, New spray chamber for use in flow injection plasma emission spectrometry, Anal. Chim. Acta 286 (1994) 155–167.

[17] J.L. Todolí, L. Gras, V. Hernandis, J. Mora, Elemental matrix effects in ICP-AES, J. Anal. At. Spectrom. 17 (2002) 142–169.

[18] C. Dubuisson, E. Poussel, J.M. Mermet, Comparison of axially and radially viewed inductively coupled plasma atomic emission spectrometry in terms of signal-to-background ratio and matrix effects, J. Anal. At. Spectrom. 12 (1997) 281–286.

[19] J.P. Rybarczyk, C.P. Jester, D.A. Yates, S.R. Koirtyohann, Spatial profiles of interelement effects in the inductively coupled plasma, Anal. Chem. 54 (1982) 2162–2170.

[20] G. Horlick, M.W. Blades, Clarification of some analyte emission characteristics of the inductively coupled plasma using emission spatial profiles, Appl. Spectrosc. 34 (1980) 229–233.

[21] K. O'Hanlon, L. Ebdon, M. Foulkes, Effect of easily ionisable elements on the mass transport efficiency of solutions and slurries used in plasma emission spectrometry, J. Anal. At. Spectrom. 12 (1997) 329–331.

[22] R. Rezaaiyaan, J.W. Olesik, G.M. Hieftje, Interferences in a low-flow, low-power inductively coupled plasma, Spectrochim. Acta Part B 40 (1985) 73–83.

[23] C. Dubuisson, E. Poussel, J.L. Todolí, J.M. Mermet, Effect of sodium during the aerosol transport and filtering in inductively coupled plasma atomic emission spectrometry, Spectrochim. Acta Part B 53 (1998) 593–600.

[24] R.K. Skogerboe, S.J. Freeland, Experimental characterization of aerosol production, transport, vaporization,

and atomization systems. Part I: factors controlling aspiration rates, Appl. Spectrosc. 39 (1985) 916–920.

[25] R.K. Skogerboe, S.J. Freeland, Experimental characterization of aerosol production, transport, vaporization, and atomization systems. Part II: factors controlling aerosol size distributions produced, Appl. Spectrosc. 39 (1985) 920–925.

[26] J.A. Borowiec, A.W. Boorn, J.H. Pillard, M.S. Cresser, R.F. Browner, M.J. Matteson, Interference effect from aerosol ionic redistribution in analytical atomic spectrometry, Anal. Chem. 52 (1980) 1054–1059.

[27] Q. Xu, D. Balik, G.R. Agnes, Aerosol static electrification and its effects in inductively coupled plasma spectroscopy, J. Anal. At. Spectrom. 16 (2001) 715–723.

[28] Q. Xu, G. Mattu, G.R. Agnes, Influence of droplets with net charge in inductively coupled plasma atomic emission spectroscopy and implications for the easily ionizable element chemical matrix effect, Appl. Spectrosc. 53 (1999) 965–973.

[29] Q. Xu, G.R. Agnes, Use of laser light scatter signals to study the effect of a DC biased mesh screen in a spray chamber on aerosols generated for use in atomic spectroscopy, Appl. Spectrosc. 54 (2000) 94–98.

[30] B.L. Sharp, Pneumatic nebulisers and spray chambers for inductively coupled plasma spectrometry. A review. Part 2: spray chambers, J. Anal. At. Spectrom. 3 (1988) 939–963.

[31] M.S. Cresser, R.F. Browner, A method for investigating size distributions of aqueous droplets in the range 0.5–10 μm produced by pneumatic nebulizers, Spectrochim. Acta Part B 35 (1980) 73–79.

[32] I.I. Stewart, J.W. Olesik, Transient acid effects in inductively coupled plasma optical emission spectrometry and inductively coupled plasma mass spectrometry, J. Anal. At. Spectrom. 13 (1998) 843–854.

[33] S. Maestre, J. Mora, J.L. Todolí, A. Canals, Evaluation of several commercially available spray chambers for use in inductively coupled plasma atomic emission spectrometry, J. Anal. At. Spectrom. 14 (1999) 61–68.

[34] J.L. Todolí, S. Maestre, J. Mora, A. Canals, V. Hernandis, The role of the spray chamber in inductively coupled plasma atomic emission spectrometry at very low liquid flow rates, Fresenius J. Anal. Chem. 368 (2000) 773–779.

[35] J.W. Olesik, J.A. Kinzer, B. Harkleroad, Inductively coupled plasma optical emission spectrometry using nebulizers with widely different sample consumption rates, Anal. Chem. 66 (1994) 2022–2030.

[36] A.H. Lefebvre, Atomization and Sprays Hemisphere Publishing Corporation, New York, 1989.

[37] Malvern Instruments, 2600 Laser Diffraction User Manual, Malvern, 1987.

[38] J.W. Olesik, L.C. Bates, Characterization of aerosols produced by pneumatic nebulizers for inductively coupled plasma sample introduction. Effect of liquid and gas flow rates on volume based drop size distributions, Spectrochim. Acta Part B 50 (1995) 285–303.

[39] J.W. Olesik, Federation of Analytical Chemistry an Spectroscopy Societies, FACSS, Detroit, Michigan, Paper # 49, 2001.

[40] J.L. Todolí, J.M. Mermet, Influence of the spray chamber design on vapor-based liquid sample introduction at room temperature in ICP-AES, J. Anal. At. Spectrom. 17 (2002) 211–218.

[41] J.M. Mermet, Use of magnesium as a test element for inductively coupled plasma atomic emission-spectrometry diagnostics, Anal. Chim. Acta 250 (1991) 85–94.

[42] E.H. van Veen, M.T.C. de Loos-Vollebregt, On the use of line intensity ratios and power adjustments to control matrix effects in inductively coupled plasma optical emission spectrometry, J. Anal. At. Spectrom. 14 (1999) 831–838.

[43] M. Stepan, P. Musil, E. Poussel, J.M. Mermet, Matrix-induced shift effects in axially viewed inductively coupled plasma atomic emission spectrometry, Spectrochim. Acta Part B 56 (2001) 443–453.

[44] I. Novotny, J.C. Fariñas, W. Jia-Liang, E. Poussel, J.M. Mermet, Effect of power and carrier gas flow on the tolerance of water loading in inductively coupled plasma atomic emission spectrometry, Spectrochim. Acta Part B 51 (1996) 1517–1526.

[45] J.L. Todolí, J.M. Mermet, Evaluation of a direct injection high-efficiency nebulizer (DIHEN) in reference to a high-efficiency nebulizer (HEN) coupled to a cyclonic spray chamber as a liquid sample introduction system for ICP-AES, J. Anal. At. Spectrom. 16 (2001) 514–520.

[46] G. Légère, E.D. Salin, Fast-clearing spray chamber for ICP-AES, Appl. Spectrosc. 48 (1994) 761–765.

[47] I.I. Stewart, J.W. Olesik, The effect of nitric acid concentration and nebulizer gas flow rates on aerosol properties and transport rates in inductively coupled plasma sample introduction, J. Anal. At. Spectrom. 13 (1998) 1249–1256.

[48] J.L. Todolí, J.M. Mermet, Acid interferences in atomic spectrometry: analyte signal effects and subsequent reduction, Spectrochim. Acta Rev. 54 (1999) 895–929.

[49] S. Maestre, J. Mora, L. Gras, J.L. Todolí, Study of the matrix effects produced by inorganic species in inductively coupled plasma atomic emission spectrometry with several spray chambers, Can. J. Anal. Sci. Spectrosc. 45 (2000) 124–132.

[50] F.J.M.J. Maessen, J. Balke, J.L.M. De Boer, Preservation of accuracy and precision in the analytical practice of low-power ICP-AES, Spectrochim. Acta Part B 37 (1982) 517–526.

[51] M. Carré, K. Lebas, M. Marichy, M. Mermet, E. Poussel, J.M. Mermet, Influence of the sample introduction system on acid effects in inductively-coupled plasma-atomicemission-spectrometry, Spectrochim. Acta Part B 50 (1995) 271–283.
[52] R.I. Botto, Method for correcting for acid and salt matrix interferences in ICP-AES, Spectrochim. Acta Part B 40 (1985) 397–412.
[53] J.L. Todolí, J.M. Mermet, Effect of the spray chamber design on steady and transient acid interferences in inductively coupled plasma atomic emission spectrometry, J. Anal. At. Spectrom. 15 (2000) 863–867.